Available online at www.sciencedirect.com
ScienceDirect
Energy Conversion and Management 48 (2007) 2103–2109
ENERGY CONVERSION & MANAGEMENT
www.elsevier.com/locate/enconman

Simulation of temperature distribution in cylindrical and prismatic lithium ion secondary batteries

Y. Inui *, Y. Kobayashi, Y. Watanabe, Y. Watase, Y. Kitamura

Department of Electrical and Electronic Engineering, Toyohashi University of Technology, Tempaku-cho, Toyohashi 441-8580, Japan

Received 21 June 2006; accepted 24 December 2006
Available online 20 February 2007

Abstract

The authors develop two-dimensional and three-dimensional simulation codes of the transient response of the temperature distribution in the lithium ion secondary battery during a discharge cycle. At first, a two-dimensional simulation code for a cylindrical battery is developed, and the simulation results for a commercially available small size battery are compared with the corresponding experimental results. The simulation results of the transient temperature and voltage variations coincide very well with the experimental results. The simulation result of the temperature difference between the center of the battery body and the center of the battery side is also in reasonable agreement with the experimental result. Next, the authors develop a three-dimensional simulation code and perform numerical simulations for three large size prismatic batteries with the same capacity and different cross sectional shapes. It is made clear that selecting the battery with the laminated cross section has a remarkable effect on the suppression of the temperature rise in comparison with the battery with square cross section, whereas the effect of the lamination on the suppression of the temperature unevenness is unexpectedly small. These results indicate the accuracy and usefulness of the developed simulation codes.

Keywords: Lithium ion secondary battery; Cylindrical cell; Prismatic cell; Temperature distribution

1. Introduction

Small size lithium ion secondary batteries are commercially available and widely used as power sources for portable electronic devices. Since the power density and current efficiency of the batteries are very high, their scale up and application as power sources for electric and hybrid vehicles, etc. are now strongly expected [1].

When the battery is enlarged, the internal heat generation becomes large, leading to the temperature rise and the occurrence of an uneven temperature distribution in the battery. The temperature rise promotes the degradation of the battery, and there exists a possibility that the uneven temperature distribution induces partial degradation in the battery [1,2]. The transient variation of the temperature distribution in the battery during its operation, therefore, should be taken into consideration to develop large size lithium ion secondary batteries.

Concerning the scale up of the lithium ion secondary batteries, up to now, many researches and developments have been reported [3,4]. The temperature distribution in the battery, however, has not yet received attention in the design process in spite of its importance. This is mainly because there exist very few simulation codes that can calculate the transient variation of the temperature distribution in the lithium ion secondary battery. So far, only several one-dimensional simulation codes considering only the radial direction of the cylindrical battery have been reported [5,6], and no two-dimensional nor three-dimensional codes has been developed.

Considering the above backgrounds, in this paper, the authors develop the two-dimensional and three-dimensional simulation codes of the transient response of the temperature distribution in the lithium ion secondary battery during a discharge cycle.

* Corresponding author. Tel.: +81 532 44 6723; fax: +81 532 44 6757.
E-mail address: inui@eee.tut.ac.jp (Y. Inui).

0196-8904/$ - see front matter © 2007 Elsevier Ltd. All rights reserved.
doi:10.1016/j.enconman.2006.12.012

Since the cylindrical shape is most popular for the commercially available small size batteries, at first, the authors develop a simulation code for this shape battery. In this case, the symmetry of the battery shape is utilized by adopting cylindrical coordinates, and the two-dimensional time dependent temperature distribution in the battery considering the battery radial and height directions is calculated. To make clear the accuracy of the code, numerical simulations are performed for a commercially available small size battery, and the calculation results are compared with the corresponding experimental results.

Prismatic batteries have an advantage in comparison with cylindrical batteries when combining them in cell modules. In the case of the prismatic battery, however, a three-dimensional simulation code is needed to calculate the temperature distribution in the battery. As a next step, the authors, therefore, develop a three-dimensional time dependent simulation code of the temperature distribution in the battery. This code adopts rectangular coordinates and can analyze prismatic batteries. The usefulness of the code is confirmed through the numerical simulations for three large size prismatic batteries with the same capacity and different cross sectional shapes.

2. Heat generation in lithium ion secondary battery

Since the transient temperature rise of the lithium ion secondary battery originates in its internal heat generation during its operation, a precise estimation of this internal heat generation is indispensable to calculate the temperature distribution with high accuracy. In this section, therefore, the authors explain the estimation method of the internal heat generation in the lithium ion secondary battery used in this study.

2.1. Mechanism of heat generation

The anode and cathode materials used in the usual lithium ion secondary batteries are lithium cobalt oxide and graphite, respectively, and the chemical reactions in this battery are expressed as the following chemical formulas [7]:

- Positive electrode reaction

$$CoO_2 + Li^+ + e^- \leftrightarrow LiCoO_2 \quad (1)$$

- Negative electrode reaction

$$LiC_6 \leftrightarrow C_6 + Li^+ + e^- \quad (2)$$

- Total reaction

$$CoO_2 + LiC_6 \leftrightarrow LiCoO_2 + C_6 \quad (3)$$

In these chemical formulas, the reactions proceed from the left side to the right side during the discharge cycle.

Assuming that ΔH, ΔG and ΔS represent the enthalpy change, Gibbs free energy change and entropy change, respectively, per unit mole of lithium ion through the above discharge reaction under the condition of constant temperature T, the following equation holds [7]:

$$\Delta H = \Delta G + T\Delta S \quad (4)$$

Since ΔG in this equation is the energy that is theoretically convertible to electricity, the open voltage of the battery E_0 can be calculated by the following equation [7]:

$$E_0 = -\frac{\Delta G}{nF} \quad (5)$$

where F is the Faraday constant and n is the number of electrons participating in the reaction and is equal to 1 for the reaction formula (3). When current flows, the voltage drop occurs by the equivalent internal resistance, which is the summation of the ohmic and reaction resistances of the battery, leading to internal heat generation in the battery. On the other hand, $T\Delta S$ represents the heat absorption by the entropy change, and it also internally generates the heat because it is rather negative for the discharge reaction of formula (3).

The internal heat generation in the power generation region of the lithium ion secondary battery, therefore, can be expressed as the following equation [7]:

$$q = r_i i^2 - T\Delta S\frac{i}{nF} \quad (6)$$

where q is the internal heat generation per unit volume and unit time, r_i is the internal equivalent resistance per unit volume and i is the discharge current per unit volume.

2.2. Measurement of internal equivalent resistance and entropy change

Since different kinds of lithium ion secondary batteries have different values of the internal equivalent resistance and the entropy change, their data should be measured beforehand to perform the numerical simulations. In this section, therefore, the authors briefly explain the method of their measurements [7] and, for example, show their measured data for the commercially available small size battery of SONY-US18650G3. This experimentally used battery is of the cylindrical spiral type, and its nominal capacity, nominal voltage, diameter and height are 1.8 A h, 3.6 V, 18 mm and 65 mm, respectively.

Since the internal equivalent resistance depends on both the temperature and SOC (state of charge) of the battery, it should be measured in various conditions with different values of the temperature and SOC. To perform efficiently this troublesome work, the authors at first measure the transient variations of the cell voltage for constant current discharge under the constant temperature condition for various values of the current and temperature and then draw many voltage–current characteristic curves by connecting the data corresponding to the same temperature and SOC. The internal equivalent resistance of the whole battery under each condition can be determined from the

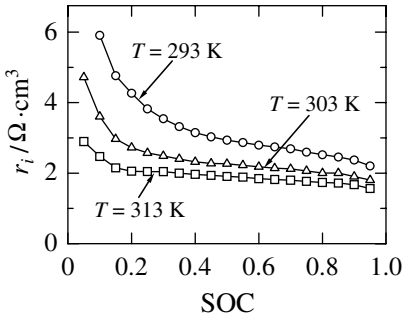

Fig. 1. Measured result of internal equivalent resistance per unit volume.

slope of the corresponding voltage–current characteristic [7], and the resistance per unit volume is obtained by using the volume of the battery power generation region. Fig. 1 shows the measured data of this internal equivalent resistance per unit volume. It can be seen that this resistance varies largely depending upon the temperature and SOC of the battery. In the developed simulation code, therefore, this resistance is utilized as the function of both temperature and SOC.

The entropy change ΔS can be obtained by measuring the dependence of the battery open voltage on the temperature because the equation:

$$\Delta S = nF\frac{\partial E_0}{\partial T} \tag{7}$$

holds according to the theory of thermodynamics. In the present study, the changes of open circuit voltage are measured for the experimentally used battery in the cases when the temperature changes from 283 to 293 K, from 293 to 303 K and from 303 to 313 K under various SOC conditions, and the entropy change is estimated from these measured finite differences of the open circuit voltage [7]. Fig. 2 depicts the obtained data of this entropy change. It can be seen that this entropy change is determined by the SOC almost regardless of the temperature. In the developed simulation code, therefore, this entropy change is incorporated as the function of only the SOC.

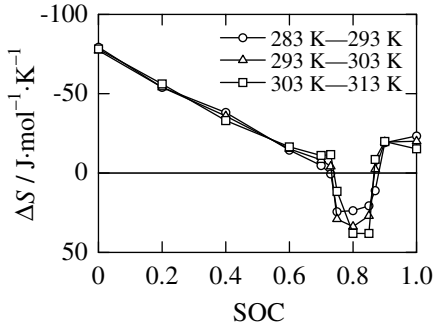

Fig. 2. Measured result of entropy change.

3. Two-dimensional simulation for cylindrical battery

Since the cylindrical shape is most popular in the commercially available small size batteries and the experimentally used battery in the present study also has this shape, the authors at first develop a simulation code of the transient response of the temperature distribution for this shape battery and compare the simulation results with the experimental results. In this case, the two-dimensional time dependent temperature distribution in the battery, considering the battery radial and height directions, is calculated because the symmetry of the battery shape can be utilized by adopting cylindrical coordinates.

3.1. Simulation method of two-dimensional analysis

Fig. 3 illustrates the schematic diagram of the cylindrical lithium ion secondary battery and the cylindrical coordinates adopted in the present simulation. The analytical region is the r–z cross section of the battery, and it is also indicated in the figure.

To simplify the simulation, the effect of the detailed spiral structure of the battery sheet on the distributions of the electrical properties is assumed to be negligible, and the power generation region of it is considered to be an assembly of identical infinitely small batteries electrically connected in parallel, while the anisotropy of the thermal conductivity from the effect of the spiral structure is taken into account because its difference along and across the battery sheet is very large and cannot be neglected [8].

Taking the above simplifications into account, the following equations can be used to calculate the transient response of the temperature distribution in the cylindrical battery:

- Power generation region

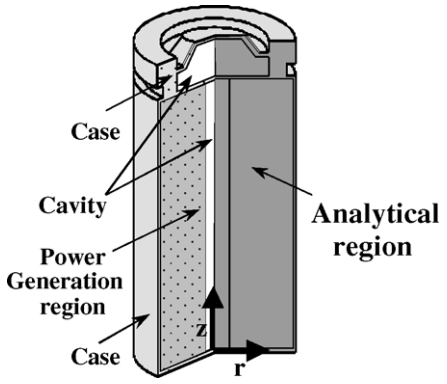

Fig. 3. Schematic diagram of cylindrical lithium ion secondary battery and analytical region.

$$\rho c\frac{\partial T}{\partial t}=\frac{1}{r}\frac{\partial}{\partial r}\left(\lambda_r r\frac{\partial T}{\partial r}\right)+\frac{\partial}{\partial z}\left(\lambda_z\frac{\partial T}{\partial z}\right)+q \tag{8}$$

$$\frac{\mathrm{d}s}{\mathrm{d}t}=-\frac{i}{c_\mathrm{i}} \tag{9}$$

$$i=\frac{E_0-E}{r_\mathrm{i}} \tag{10}$$

$$I=\int\int_S 2\pi r i\,\mathrm{d}r\,\mathrm{d}z \tag{11}$$

- Case and cavity

$$\rho c\frac{\partial T}{\partial t}=\frac{1}{r}\frac{\partial}{\partial r}\left(\lambda_r r\frac{\partial T}{\partial r}\right)+\frac{\partial}{\partial z}\left(\lambda_z\frac{\partial T}{\partial z}\right) \tag{12}$$

where s is the local state of charge, E is the terminal voltage, I is the discharge current, ρ is the mass density, c is the specific heat, λ is the thermal conductivity, c_i is the capacity per unit volume of the power generation region, S is the power generation region on the r–z plane and the subscripts r and z denote the values along the r- and z-directions, respectively.

In addition, the battery is assumed to be cooled by natural convection of the ambient air. In this case, the heat flux q_f from the battery surface to the air can be calculated by the following equation [7]:

$$q_\mathrm{f}=h(T-T_0) \tag{13}$$

where T_0 is the ambient temperature and h is the heat transfer coefficient. This heat flux is employed as the boundary condition on the battery surface required for calculation of the temperature distribution.

The developed simulation code calculates the transient response of the temperature distribution in the battery along with the transient responses of the current distribution, state of charge distribution and terminal voltage for given discharge current by solving the above equations simultaneously.

3.2. Numerical conditions

The commercially available small size cylindrical lithium ion secondary battery of SONY-US18650G3, which has already been used in the previous section, is also used in the experiments of the transient temperature response. The simulations are, therefore, performed for this battery to make the comparison between the simulation results and experimental results possible.

As for the internal equivalent resistance r_i and the entropy change ΔS, the measured data shown in the previous section are employed. In the code, r_i is taken as the function of both the state of charge s and the temperature T, and ΔS is taken as the function of s.

The product of the mass density and the specific heat ρc is the heat capacity per unit volume, and in the power generation region, it is selected as 1.83 MJ/(m^3 K) [7]. Since the heat easily conducts along the battery sheet rather than across the sheet, the anisotropy of the thermal conductivity λ is taken into account for the power generation region, and the values of 1.09 and 3.82 W/(m K) are chosen as λ_r and λ_z, respectively [8]. The case and cavity are assumed to be isotropic and be composed of stainless steel and air, respectively, and their values of mass density, specific heat and thermal conductivity are used for these regions. The heat transfer coefficient h is selected as 8.0 W/(m^2 K) [7], because this is the standard value corresponding to natural convection cooling by ambient air.

3.3. Simulation results

Numerical simulations of the transient responses of the temperature distribution in the battery are performed for 0.9 A (0.5 C) and 1.8 A (1.0 C) constant current discharges. In the calculations, the authors assume that the battery is initially under the full charge condition and the discharge is continued until the SOC reaches 0.1. The calculation results are compared with the corresponding experimental results.

Figs. 4 and 5 depict the experimentally and numerically obtained transient variations of the temperature at the center of the battery side and the cell voltage for 0.9 A and 1.8 A, respectively. In these figures, the time passage is expressed by the variation of the SOC because it linearly decreases in the case of the constant current discharge. From these figures, it can be confirmed that the simulation results of the transient temperature and voltage variations coincide very well with the experimental results for both the 0.9 A and 1.8 A constant current discharge.

Since the temperature measurement inside the battery inevitably breaks its seal and causes very rapid degradation of its performance, the authors measure the temperature at the center of the battery body only once. This measurement is performed for the 1.8 A discharge. It is made clear that the measured temperature at the battery center is higher than that at the battery side, and the temperature difference is 0.8 K at the end of the discharge. As for the simulation result, Fig. 6 illustrates the temperature distribution in the battery at the end of the 1.8 A constant current discharge. As shown in this figure, the numerically obtained temperature difference corresponding to the experiment is

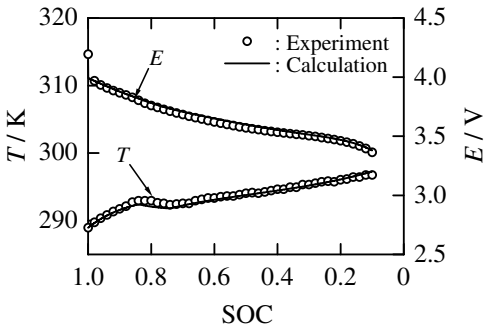

Fig. 4. Experimentally and numerically obtained transient temperature and voltage variations of cylindrical battery for 0.9 A constant current discharge.

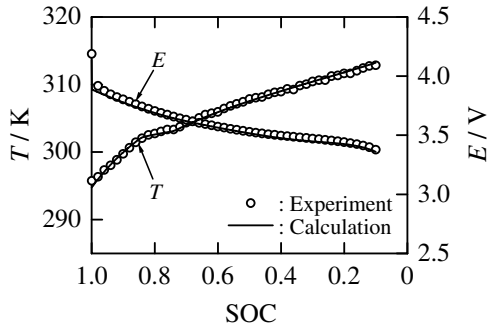

Fig. 5. Experimentally and numerically obtained transient temperature and voltage variations of cylindrical battery for 1.8 A constant current discharge.

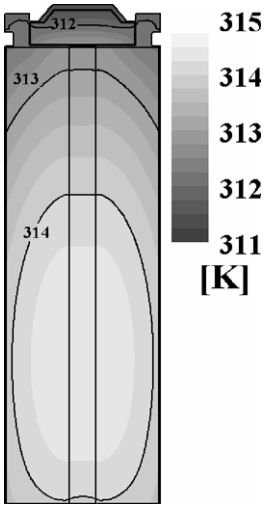

Fig. 6. Numerically obtained temperature distribution in cylindrical battery at end of 1.8 A constant current discharge.

0.6 K, and reasonable agreement with the experimental result is successfully obtained.

The above results indicate the accuracy of the developed simulation code of the transient response of the temperature distribution in the lithium ion secondary battery.

4. Three-dimensional simulation for prismatic battery

Prismatic batteries have an advantage in comparison with cylindrical batteries in combining them as cell modules. In the case of the prismatic battery, however, a three-dimensional simulation code is needed to calculate the temperature distribution in the battery. As a next step, the authors, therefore, develop a three-dimensional time dependent simulation code of the temperature distribution in the battery. This code adopts rectangular coordinates and can analyze prismatic batteries.

4.1. Simulation method of three-dimensional analysis

Fig. 7 shows the schematic diagram of the prismatic lithium ion secondary battery and the rectangular coordinates

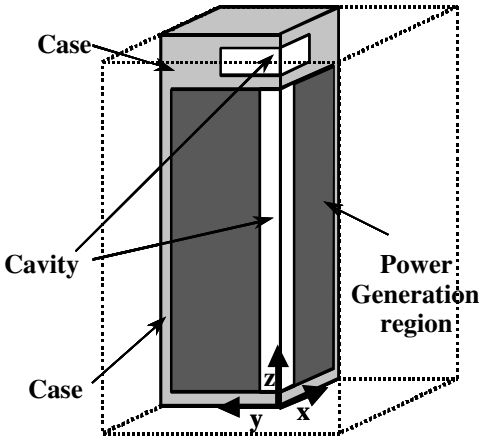

Fig. 7. Schematic diagram of prismatic lithium ion secondary battery and analytical region.

adopted in this simulation, where the x-, y- and z-axes are fixed along the battery length, width and height directions, respectively, and the origin is located at the center of the battery bottom surface. Considering the symmetry of the battery shape, the one quarter part of it indicated in the figure is selected as the analytical region.

Taking the same simplifications assumed in the above explained two-dimensional simulation code into account, the following equations can be used to calculate the transient response of the temperature distribution in the prismatic battery:

- Power generation region

$$\rho c\frac{\partial T}{\partial t}=\frac{\partial}{\partial x}\left(\lambda_x\frac{\partial T}{\partial x}\right)+\frac{\partial}{\partial y}\left(\lambda_y\frac{\partial T}{\partial y}\right)+\frac{\partial}{\partial z}\left(\lambda_z\frac{\partial T}{\partial z}\right)+q \tag{14}$$

$$\frac{\mathrm{d}s}{\mathrm{d}t}=-\frac{i}{c_\mathrm{i}} \tag{15}$$

$$i=\frac{E_0-E}{r_\mathrm{i}} \tag{16}$$

$$I=4\int\int\int_V i\,\mathrm{d}x\,\mathrm{d}y\,\mathrm{d}z \tag{17}$$

- Case and cavity

$$\rho c\frac{\partial T}{\partial t}=\frac{\partial}{\partial x}\left(\lambda_x\frac{\partial T}{\partial x}\right)+\frac{\partial}{\partial y}\left(\lambda_y\frac{\partial T}{\partial y}\right)+\frac{\partial}{\partial z}\left(\lambda_z\frac{\partial T}{\partial z}\right) \tag{18}$$

- Heat flux from battery surface

$$q_\mathrm{f}=h(T-T_0) \tag{19}$$

where V is the power generation region in the analytical region, and the subscripts x, y and z denote the values along the x-, y- and z-directions, respectively.

In the same manner as the two-dimensional code, the three-dimensional code calculates the transient response of the temperature distribution in the battery along with the transient responses of the current distribution, state of charge distribution and terminal voltage for given discharge current by solving the above equations simultaneously.

4.2. Numerical conditions

The accuracy of the simulation has already been confirmed in the previous section through the experiments and two-dimensional calculations of the commercially available small size cylindrical battery. Different from the cylindrical battery, various cross sectional shapes can be selected for the same battery height and capacity in the case of the prismatic battery. Considering these facts, in this section, the authors assume three models of large size prismatic batteries with different cross sectional shapes and the same capacity, and investigate the influence of the shape on the transient response of the temperature distribution through the three-dimensional calculations.

As the battery sheet, the same one contained in the experimentally used small size battery is selected in the present simulations. The capacity is fixed as 9.0 A h, and the sizes (length × width × height) of the three model batteries are chosen as follows: 34.4 mm × 34.4 mm × 68.8 mm for Model 1 battery, 68.8 mm × 17.2 mm × 68.8 mm for Model 2 battery and 137.6 mm × 8.6 mm × 68.8 mm for Model 3 battery. All these model batteries have the same height and volume, and the volume is enlarged fivefold in comparison with the experimentally used battery corresponding to the enlargement of the capacity by five times. The Model 1 battery has a square cross section. The Model 3 battery is rather a laminated shape and this shape is also promising for future large size batteries.

Since the same battery sheet is assumed, the same data of the internal equivalent resistance, entropy change, heat capacity per unit volume, thermal conductivity and heat transfer coefficient used in the previous section are also employed in the present simulations.

4.3. Simulation results

Numerical simulations of the transient responses of the temperature distribution in the three model batteries are performed for 9.0 A (1.0 C) constant current discharge. In the calculations, the authors assume that the battery is initially under the full charge condition, and the discharge is continued until the SOC reaches 0.1.

Fig. 8 depicts the numerically obtained transient variations of the highest temperature in these three model batteries. This figure tells that the temperature rise during the discharge becomes different depending upon the cross sectional shape even under the condition of the same battery volume and capacity, and selecting the battery with the laminated cross section, such as Model 3, has a remarkable effect on suppression of the temperature rise in comparison with the battery with the square cross section, such as Model 1. This result is considered to be caused by the difference in the surface area of these three model batteries because the cooling effect by the ambient air is proportional to the surface area, and the Model 3 battery with laminated cross section has the largest surface area.

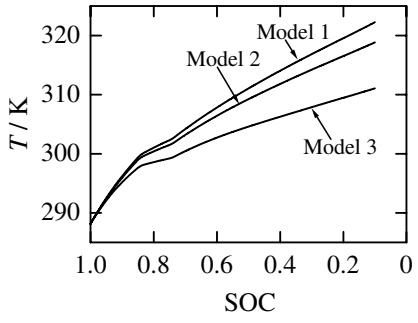

Fig. 8. Numerically obtained transient variations of highest temperature in prismatic batteries.

As for the temperature distributions at the end of the discharge, those on the x–z plane at $y = 0$ and on the y–z plane at $x = 0$ for the three model batteries are illustrated in Figs. 9–11. It is made clear that the unevenness of the temperature distribution in the battery is not very different among the three model batteries, and the effect of the lamination on the suppression of the temperature unevenness is unexpectedly small. Some other measure is, therefore, considered to be needed to suppress this unevenness.

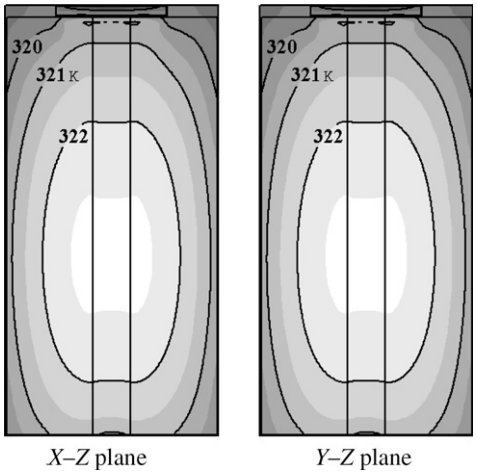

Fig. 9. Numerically obtained temperature distribution in Model 1 type prismatic battery at end of 9.0 A constant current discharge.

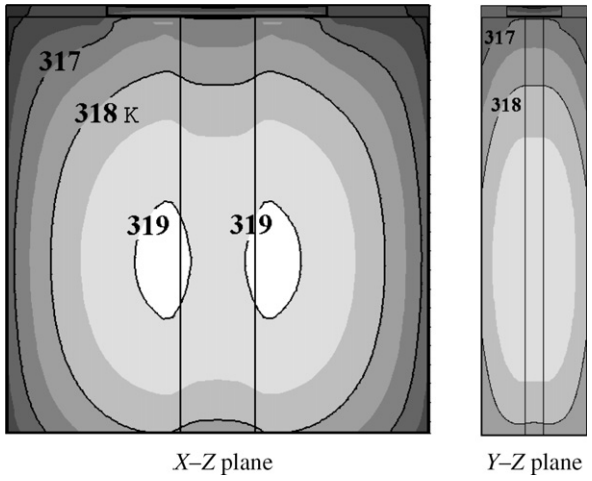

Fig. 10. Numerically obtained temperature distribution in Model 2 type prismatic battery at end of 9.0 A constant current discharge.

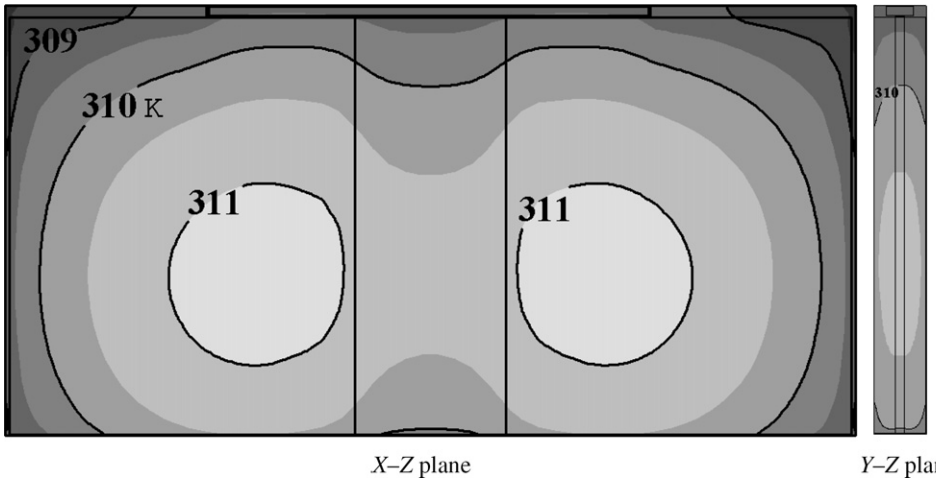

Fig. 11. Numerically obtained temperature distribution in Model 3 type prismatic battery at end of 9.0 A constant current discharge.

The obtained results are very informative to determine the cross sectional shape of large size batteries. In addition, the above simulation is only an example, and the developed three-dimensional code is expected to be applicable for various kinds of simulations required in the design process of large size batteries, indicating the usefulness of the developed simulation code of the transient response of the temperature distribution in the lithium ion secondary battery.

5. Conclusions

In this paper, the authors develop two-dimensional and three-dimensional simulation codes of the transient response of the temperature distribution in the lithium ion secondary battery during a discharge cycle.

At first, the authors develop a two-dimensional simulation code for cylindrical batteries. In this case, the symmetry of the battery shape is utilized by adopting cylindrical coordinates, and the two-dimensional time dependent temperature distribution in the battery, considering the battery radial and height directions, is calculated. Numerical simulations are performed for a commercially available small size battery, and the calculation results are compared with the corresponding experimental results. The simulation results of the transient temperature and voltage variations coincide very well with the experimental results. As for the temperature difference between the center of the battery body and the center of the battery side, the simulation result is also in reasonable agreement with the experimental result. These results indicate the accuracy of the developed simulation code of the transient response of the temperature distribution in the lithium ion secondary battery.

Next, the authors developed a three-dimensional simulation code. This code adopts rectangular coordinates and can analyze the three-dimensional time dependent temperature distribution in prismatic batteries. Numerical simulations for three large size prismatic batteries with the same capacity and different cross sectional shapes are performed. It is made clear that the temperature rise during discharge becomes different depending upon the cross sectional shape even under the condition of the same battery volume and capacity, and selecting the battery with the laminated cross section has a remarkable effect on the suppression of the temperature rise in comparison with the battery with the square cross section. The effect of the lamination on the suppression of the temperature unevenness is, however, unexpectedly small, and some other measure is considered to be needed to suppress this unevenness. These results are very informative to determine the cross sectional shape of large size batteries. In addition, this simulation is only an example, and the developed three-dimensional code is expected to be applicable for various kinds of simulations required in the design process of large size batteries, indicating the usefulness of the developed simulation code of the transient response of the temperature distribution in the lithium ion secondary battery.

References

[1] Sato N, Sakai T. Large scale rechargeable batteries for vehicles. CMC Publishing; 2003 [in Japanese].
[2] Kanemura K. Lithium secondary battery technology for the 21st century. CMC Publishing; 2004 [in Japanese].
[3] Kojima T, Shiozaki R, Okamoto K, Okabe K, Ono T. Development of 100 A h manganese-type lithium-ion battery. In: 42nd battery symposium in Japan, 2001. p. 440–1 [in Japanese].
[4] Nakamoto T, Seyama Y, Nishiyama K, Sonoda T. Development of large-scale lithium ion batteries for high power industrial applications. In: 46th battery symposium in Japan, 2005. p. 520–1 [in Japanese].
[5] Takano K, Hirayama T, Nakano T. Simulation of electrical characteristics in a large-capacity lithium secondary battery. Bull Electrotechn Lab 1996;60:817–24 [in Japanese].
[6] Al Hallaj S, Maleki H, Hong JS, Selman JR. Thermal modeling and design considerations of lithium-ion batteries. J Power Sour 1998;83:1–8.
[7] Kameyama H, Hanamoto T, Ito K, Inui Y, Onda K. Study on heat generation behavior of small lithium-ion secondary battery. Trans IEE Jpn 2002;122-B:1192–9 [in Japanese].
[8] Kanari K, Takano K, Saito Y. Thermal behavior and simulation of a lithium secondary battery. Bull Electrotechn Lab 1996;60:825–35.